

Multi-path vector entanglement engineering via dark mode control in optomechanics

P. Djourwé,^{1,2,*} R. Altujiri,^{3,†} A. J. Almalki,^{4,‡} S. Abdel-Khalek,^{5,§} and A.-H. Abdel-Aty^{6,¶}

¹*Department of Physics, Faculty of Science, University of Ngaoundere, P.O. Box 454, Ngaoundere, Cameroon*

²*Stellenbosch Institute for Advanced Study (STIAS), Wallenberg Research Centre at Stellenbosch University, Stellenbosch 7600, South Africa*

³*Department of Physics, College of Science, Princess Nourah bint Abdulrahman University, P.O. Box 84428, Riyadh 11671, Saudi Arabia*

⁴*Department of Computer Science and Artificial Intelligence,*

College of Computing and Information Technology, University of Bisha, Bisha 61922, Saudi Arabia

⁵*Department of Mathematics and Statistics, College of Science,*

Taif University, P.O. Box 11099, 21944, Saudi Arabia

⁶*Department of Physics, College of Sciences, University of Bisha, Bisha 61922, Saudi Arabia*

We propose a scheme to generate multi-paths entanglement in an optomechanical system by exploiting polarized electromagnetic fields and dark mode control. Our system consists of two mechanically coupled mechanical resonators, which are driven by a common electromagnetic field. An inclusion of a polarizer induces linear polarizations of the electromagnetic field corresponding to the vertical (transverse electric (TE) and horizontal (transverse magnetic [(TM)) modes, which drive the mechanical resonators. Without the mechanical coupling $J_m = 0$, the polarization angle (ϕ) controls dark mode in the system. The breaking of this dark mode leads to multi-paths engineering of bipartite optomechanical entanglements. By switching on the phonon hopping rate ($J_m \neq 0$), both the polarization angle and the modulation phase of the mechanical coupling allow a further control of the dark mode. The simultaneous Dark Mode Breaking (DMB) conditions under these two parameters leads to multi-paths bipartite and tripartite entanglements. For a fine tuning of the polarization angle ($\phi = \pi/4$) this scheme enables a generation of twin entangled states, where the bipartite/tripartite generated entangled states are degenerated and might be of great interest for quantum information processing, quantum communication and diverse quantum computational tasks. The generated entanglements are more resilient against thermal fluctuations in the DMB regime, i.e., up to two order of magnitude robust than in the Unbreaking regime. Our work sheets light on new possibilities to generate noise-tolerant quantum resources that are useful for plethora of modern quantum technologies.

Keywords: Entanglement, optomechanics, polarization, dark mode

I. INTRODUCTION

Quantum entanglement is an interesting and vital resource for modern quantum technologies including quantum information processing [1, 2], quantum metrology [3, 4] and sensing [5–8], quantum communication protocols [9–11], and quantum computational tasks [12–14], just to name few. However, generating such non-classical states is not an easy task, since they require specific engineering schemes for their stabilization [15, 16] against thermal fluctuations and other external environmental perturbations during their processing. Several way of generating stable an robust entangled states have been proposed in different fields, for instance in plasmonic systems [17], electron spin systems [18], superconducting circuits [19–21], and optomechanics [22].

Different optomechanical structures have been recently used as benchmark systems to generate quantum entanglements. Optomechanical entanglement, i.e., entanglement between electromagnetic field and center of mass of a mechanical object has been firstly investigated in [23]. Later on, other interesting works on entanglement involving optomechanical systems and hybrid related systems have been re-

alized both theoretically and experimentally. Owing to their vulnerability against environmental disturbances, entangled states are fragile for certain applications. To handle such an issue, number of studies on macroscopic entanglement have been realized. A stabilization of macroscopic entanglement of two massive micromechanical oscillators have been achieved in [24], where the mechanical oscillators were coupled to a microwave-frequency electromagnetic cavity. A pulsed electromechanical system has led to a direct entanglement observation of two mechanical drumheads through quantum state tomography in [25]. Similarly, a Duan quantity of 1.4 decibels below the separability bound has been measured [26], revealing quantum entanglement of two micromechanical oscillators. Beside of these interesting achievements, there are recent theoretical proposals aiming to enhance quantum entanglement. For instance, different nonlinearities have been used to improve entanglement such as Duffing nonlinearity [27], Kerr nonlinearity [28], Brillouin scattering [29, 30], and quadratic coupling [31]. Moreover, sophisticated technics based on exceptional points [32] and dark mode control have been proposed as well [33, 34]. Despite these aforementioned entanglement investigations in optomechanical structures, the urge to propose schemes that generate abundant entanglement resources is still crucial for applications involving large network of entities. Such schemes can be useful to overcome the entanglement sharing among multiple users, which remains a fundamental issue in modern quantum computational tasks. For this purposes, multipath quantum entanglement sources have been proposed [35, 36], enabling an efficient distribution of

*Electronic address: djourwepp@gmail.com

†Electronic address: raaltuwagry@pnu.edu.sa

‡Electronic address: alialmalki@ub.edu.sa

§Electronic address: asbotalb@tu.edu.sa

¶Electronic address: amabdelaty@ub.edu.sa

the quantum resources among multiuser of a multiplexed architecture [37, 38]. While some of these protocols are based on a generation of two photons by spontaneous parametric down-conversion [35, 39], and other based on segment routing/quantum repeaters [36], recent developments in optomechanics make use of polarization of electromagnetic field.

Polarization of electromagnetic field has been used to foster interesting phenomena in physics owing to the fact that the polarized fields provide extra free control parameter to the system. The induced phenomena include Faraday effect [40], chiral exceptional point polarization conversion [41], and entanglement [42], among others. In optomechanical systems, polarizations of electromagnetic field have been used to perform optomechanically induced transparency [43], phonon laser [44], and quantum entanglement [45, 46]. The entanglement polarization have been investigated so far in single optomechanical cavity (where the polarized fields interact with a mechanical resonator), and it only focuses on bipartite entanglement. In our proposal, we extend this concept to a large structure where the polarized fields interact with two mechanical resonators, and we investigated both bipartite and tripartite quantum entanglements. Our proposal can be seen as an optical cavity driven by linear polarizations of the electromagnetic field, i.e., the vertical (transverse electric (TE) and horizontal (transverse magnetic [(TM)) modes, which interact with two mechanical resonators placed within the cavity. The involved mechanical resonators are mechanically coupled through a phonon hopping rate J_m , which is θ -modulated. When the phonon hopping rate is off ($J_m = 0$), we have used the polarization angle to control dark mode in the system, and this has led to a generation of multi-path bipartite entanglements. In this case, no tripartite entanglement was engineered. As the mechanical coupling is switched on ($J_m \neq 0$), both the polarization angle (ϕ) and the modulation phase (θ) are used to control dark mode, leading to interesting outcomes. Under the simultaneous Dark Mode Breaking (DMB) conditions, i.e., realized by tuning both ϕ and θ , we have found that i) multi-paths bipartite and tripartite entanglements are generated, providing abundant quantum resources, ii) twin bipartite/tripartite entangled states are engineered for $\phi = \pi/4$, and iii) the generated entanglements are up to two order of magnitude robust against thermal noises compared to those engineered in the Unbreaking regime. Our proposal constitutes a rich platform to generate noise-tolerant quantum resources which are of great interest for quantum information processing, quantum communication network and modern quantum computational tasks.

The rest of the work is organized as follow. The model and the involved equations are described in [section II](#), together with the theoretical quantification of the entanglements. Bipartite and tripartite entanglements are investigated in [section III](#) and [section IV](#), respectively. Our conclusion is presented in [section V](#).

II. MODEL AND DYNAMICAL EQUATIONS

Our benchmark system consists of a linearly polarized electromagnetic field whose polarized components simultaneously drive two mechanical resonators. Both mechanical resonators are mechanically coupled through a phonon hopping rate J_m . This mechanical coupling is modulated through a phase θ , which can be used to induces a synthetic magnetism in the system [47, 48]. In a frame rotating with respect to the driving frequency ω_L , the Hamiltonian of our system (with $\hbar = 1$) is given by,

$$H = H_O + H_{OM} + H_{int} + H_{drive}, \quad (1)$$

with

$$\begin{cases} H_O &= -\sum_{p=\uparrow,\leftrightarrow} \Delta_p a_p^\dagger a_p + \sum_{j=1,2} \omega_j b_j^\dagger b_j, \\ H_{OM} &= \sum_{j=1,2} \left[\sum_{p=\uparrow,\leftrightarrow} g_p a_p^\dagger a_p (b_j^\dagger + b_j) \right], \\ H_{int} &= J_m \left(e^{i\theta} b_1^\dagger b_2 + e^{-i\theta} b_1 b_2^\dagger \right), \\ H_{drive} &= i\sqrt{\kappa} \sum_{p=\uparrow,\leftrightarrow} \alpha_p^{in} (a_p^\dagger + a_p), \end{cases} \quad (2)$$

where H_O , H_{OM} , H_{int} , and H_{drive} are the Hamiltonians for the free optomechanical system, the optomechanical coupling, the mechanical interaction, and the driving fields, respectively. The double arrows $\uparrow, \leftrightarrow$ denote the linear polarizations of the electromagnetic field driving the mechanical resonators. We have defined the detuning $\Delta_p = \omega_L - \omega_c^p$, with ω_c^p being the cavity frequency related to the p^{th} polarized field. The electromagnetic (mechanical) modes are captured by the annihilation a_p (b_j) and creation a_p^\dagger (b_j^\dagger) operators. The mechanical frequencies are denoted by ω_j , while g_j stands for the single-photon optomechanical coupling rate.

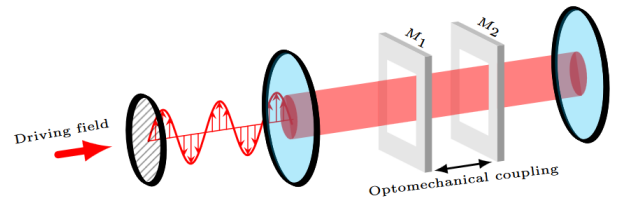


FIG. 1: Sketch of our proposal. Two mechanically coupled mechanical resonators are placed inside an optical resonator, which is driven by polarized electromagnetic fields.

The amplitude of the linearly polarized driving field is $\alpha^{in} = |\alpha_{\uparrow}^{in}|^2 + |\alpha_{\leftrightarrow}^{in}|^2$, where $\alpha_{\uparrow}^{in} = \alpha^{in} \cos \phi$ and $\alpha_{\leftrightarrow}^{in} = \alpha^{in} \sin \phi$ being the projections of α^{in} onto the vertical and horizontal modes, respectively. The driving field is related to the input power P^{in} through $\alpha^{in} = \sqrt{P^{in}/\hbar\omega_L}$. The aforementioned linear polarizations of the electromagnetic field correspond to the vertical (transverse electric [TE]) and horizontal (transverse magnetic [TM]) modes of the Fabry-Pérot cavity. These linearly polarized light can be thought as a superposition of orthogonal patterns encoded into the unit vector $|\mathbf{e}\rangle = \cos \phi |\mathbf{e}_{\uparrow}\rangle + \sin \phi |\mathbf{e}_{\leftrightarrow}\rangle$, where ϕ is the angle between

the linearly direction of the involved polarization. In such a configuration, one can coherently manipulate the spatial distribution of optical field by tuning its polarization structure through the angle ϕ . By invoking the Heisenberg equation, one can derive the following Quantum Langevin Equations (QLEs),

$$\begin{cases} \dot{a}_p &= \left\{ i \left[\Delta_p - g_p \sum_{j=1}^2 (b_j^\dagger + b_j) \right] - \frac{\kappa}{2} \right\} a_p + \sqrt{\kappa} \alpha_p^{in}, \\ \dot{b}_j &= - \left(i\omega_j + \frac{\gamma_m}{2} \right) b_j - iJ_m b_{3-j} e^{(-1)^{3-j}i\theta} - i \sum_{p=\uparrow, \leftrightarrow} g_p a_p^\dagger a_p. \end{cases} \quad (3)$$

where we have assumed the same dissipations for the polarized modes ($\kappa_\uparrow \equiv \kappa_\leftrightarrow \equiv \kappa$), and for the mechanical modes ($\gamma_1 \equiv \gamma_2 \equiv \gamma$). From now on, we will also assume that the two polarized modes couple to the mechanical resonators with the same rate ($g_\uparrow \equiv g_\leftrightarrow \equiv g$). By using the standard linearization procedure, where the operators are splitted into their mean value and some amount of fluctuations, i.e., $a_p = \alpha_p + \delta\alpha_p$ and $b_j = \beta_j + \delta\beta_j$, one gets the mean dynamical equations,

$$\begin{cases} \dot{\alpha}_p &= (i\tilde{\Delta}_p - \frac{\kappa}{2}) \alpha_p + \sqrt{\kappa} \alpha_p^{in}, \\ \dot{\beta}_j &= - \left(i\omega_j + \frac{\gamma_m}{2} \right) \beta_j - iJ_m \beta_{3-j} e^{(-1)^{3-j}i\theta} - ig \sum_{p=\uparrow, \leftrightarrow} |\alpha_p|^2, \end{cases} \quad (4)$$

and the fluctuations dynamics,

$$\begin{cases} \delta\dot{\alpha}_p &= (i\tilde{\Delta}_p - \frac{\kappa}{2}) \delta\alpha_p - ig \alpha_p \sum_{j=1}^2 (\delta\beta_j^\dagger + \delta\beta_j) + \sqrt{\kappa} \delta\alpha_p^{in}, \\ \delta\dot{\beta}_j &= - \left(i\omega_j + \frac{\gamma_m}{2} \right) \delta\beta_j - iJ_m \delta\beta_{3-j} e^{(-1)^{3-j}i\theta} \\ &\quad - ig \sum_{p=\uparrow, \leftrightarrow} \alpha_p (\delta\alpha_p^\dagger + \delta\alpha_p) + \sqrt{\gamma_m} \delta\beta_j^{in}, \end{cases} \quad (5)$$

with the effective detuning $\tilde{\Delta}_p = \Delta_p - 2g \sum_{j=1}^2 \text{Re}(\beta_j)$. We have also defined the effective couplings $G_p = g\alpha_p$, i.e., $G_\uparrow = G_m \cos \phi$ and $G_\leftrightarrow = G_m \sin \phi$, with $G_m = g\alpha_0$ corresponding to $\phi = 0$. The quantum fluctuations are captured by $\delta\alpha_p^{in}$, and

$\delta\beta_j^{in}$ which are zero-mean noise operators characterized by the following auto-correlation functions,

$$\begin{aligned} \langle \delta\alpha_p^{in}(t) \delta\alpha_p^{in\dagger}(t') \rangle &= \delta(t-t'), \\ \langle \delta\alpha_p^{in\dagger}(t) \delta\alpha_p^{in}(t') \rangle &= 0, \\ \langle \delta\beta_j^{in}(t) \delta\beta_j^{in\dagger}(t') \rangle &= (n_{th}^j + 1) \delta(t-t'), \\ \langle \delta\beta_j^{in\dagger}(t) \delta\beta_j^{in}(t') \rangle &= n_{th}^j \delta(t-t'), \end{aligned}$$

where n_{th} is the thermal phonon occupation of the mechanical resonator defined as $n_{th} = [\exp(\frac{\hbar\omega_m}{k_b T}) - 1]^{-1}$, where k_b is the Boltzmann constant.

To quantify the bipartite entanglement within our system, we need to compute the covariance matrix through the quantum quadratures. For this purpose, we introduce the following quadratures, $\delta I_p = \frac{1}{\sqrt{2}}(\delta\alpha_p + \delta\alpha_p^\dagger)$, $\delta Y_p = \frac{i}{\sqrt{2}}(\delta\alpha_p^\dagger - \delta\alpha_p)$, $\delta X_j = \frac{1}{\sqrt{2}}(\delta\beta_j + \delta\beta_j^\dagger)$ and $\delta P_j = \frac{i}{\sqrt{2}}(\delta\beta_j^\dagger - \delta\beta_j)$, together with their corresponding noise quadratures. The substitution of these quadratures into the fluctuation equations leads to the quadrature equations, which can be cast into their following compact form,

$$\delta\dot{X} = M\delta X + N\delta X^{in} \quad (6)$$

with the column vector $\delta X = (\delta I_\leftrightarrow, \delta Y_\leftrightarrow, \delta I_\uparrow, \delta Y_\uparrow, \delta X_1, \delta P_1, \delta X_2, \delta P_2)^T$, and the corresponding noise column vector $\delta X^{in} = (\delta I_\leftrightarrow^{in}, \delta Y_\leftrightarrow^{in}, \delta I_\uparrow^{in}, \delta Y_\uparrow^{in}, \delta X_1^{in}, \delta P_1^{in}, \delta X_2^{in}, \delta P_2^{in})^T$. The drift matrix N is given by $N = \text{Diag}(\sqrt{\kappa}, \sqrt{\kappa}, \sqrt{\kappa}, \sqrt{\kappa}, \sqrt{\gamma_m}, \sqrt{\gamma_m}, \sqrt{\gamma_m}, \sqrt{\gamma_m})$. In the above quadrature equations, the matrix M reads,

$$M = \begin{pmatrix} -\frac{\kappa}{2} & -\tilde{\Delta}_{\leftrightarrow} & 0 & 0 & 2\text{Im}(G_{\leftrightarrow}) & 0 & 2\text{Im}(G_{\leftrightarrow}) & 0 \\ \tilde{\Delta}_{\leftrightarrow} & -\frac{\kappa}{2} & 0 & 0 & -2\text{Re}(G_{\leftrightarrow}) & 0 & -2\text{Re}(G_{\leftrightarrow}) & 0 \\ 0 & 0 & -\frac{\kappa}{2} & -\tilde{\Delta}_\uparrow & 2\text{Im}(G_\uparrow) & 0 & 2\text{Im}(G_\uparrow) & 0 \\ 0 & 0 & \tilde{\Delta}_\uparrow & -\frac{\kappa}{2} & -2\text{Re}(G_\uparrow) & 0 & -2\text{Re}(G_\uparrow) & 0 \\ 2\text{Im}(G_{\leftrightarrow}) & 0 & 2\text{Im}(G_\uparrow) & 0 & -\frac{\gamma_m}{2} & \omega_1 & J_m \sin \theta & J_m \cos \theta \\ -2\text{Re}(G_{\leftrightarrow}) & 0 & -2\text{Re}(G_\uparrow) & 0 & -\omega_1 & -\frac{\gamma_m}{2} & -J_m \cos \theta & J_m \sin \theta \\ 2\text{Im}(G_{\leftrightarrow}) & 0 & 2\text{Im}(G_\uparrow) & 0 & -J_m \sin \theta & J_m \cos \theta & -\frac{\gamma_m}{2} & \omega_2 \\ -2\text{Re}(G_{\leftrightarrow}) & 0 & -2\text{Re}(G_\uparrow) & 0 & -J_m \cos \theta & -J_m \sin \theta & -\omega_2 & -\frac{\gamma_m}{2} \end{pmatrix}. \quad (7)$$

From the above quadrature equations, one can now define the covariance's matrix elements as $V_{ij} = \frac{\langle \delta X_i \delta X_j + \delta X_j \delta X_i \rangle}{2}$, which also satisfy the motional equation,

$$\dot{V} = MV + VM^T + D, \quad (8)$$

where the diagonal diffusion matrix is expressed as $D = \text{Diag}[\frac{\kappa}{2}, \frac{\kappa}{2}, \frac{\kappa}{2}, \frac{\kappa}{2}, \frac{\gamma_m}{2}(2n_{th}^1 + 1), \frac{\gamma_m}{2}(2n_{th}^1 + 1), \frac{\gamma_m}{2}(2n_{th}^2 + 1), \frac{\gamma_m}{2}(2n_{th}^2 + 1)]$. To be meaningful, the matrix M must satisfy the Routh-Hurwitz stability criterion, i.e., all its eigenval-

ues should have negative real parts [49]. Our used parameters have been chosen within this stability range as depicted in Figure 2. This figure displays the stability of our system versus the phonon hopping rate J_m and the effective coupling G_m . The blue/dark region captures the system parameters enabling stability, while the red/light area represents the unstable zone.

To quantify the steady-state behavior of the entanglement, we consider the long time limit of the dynamics in Equation 8, where the variable are no longer time dependent. Therefore,

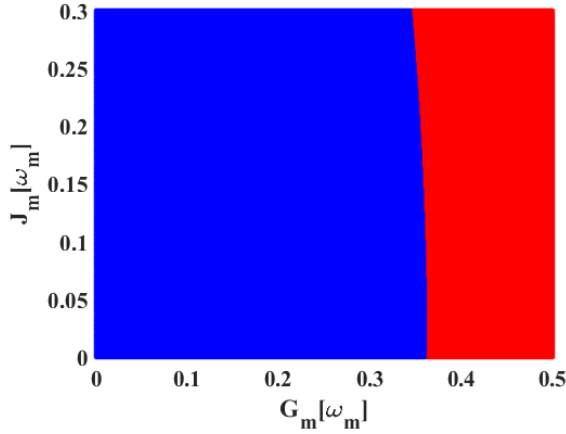


FIG. 2: Stability diagram of the system depending on the effective coupling G_m and the mechanical coupling J_m . The blue/dark region is stable, while the red/light area represents the unstable zone. The used parameters are $\tilde{\Delta} = -\omega_m$, $\kappa = 0.2\omega_m$, $\omega_j = \omega_m$, $\gamma_j = 10^{-5}\omega_m$, $\phi = \frac{\pi}{4}$, and $\theta = \frac{\pi}{2}$.

the motional equation in Equation 8 reduces to the Lyapunov equation,

$$MV + VM^T = -D, \quad (9)$$

and the covariance matrix takes the general form,

$$V = \begin{pmatrix} V_{\alpha_{\leftrightarrow}} & V_{\alpha_{\leftrightarrow}, \alpha_{\downarrow}} & V_{\alpha_{\leftrightarrow}, \beta_1} & V_{\alpha_{\leftrightarrow}, \beta_2} \\ V_{\alpha_{\leftrightarrow}, \alpha_{\downarrow}}^T & V_{\alpha_{\downarrow}} & V_{\alpha_{\downarrow}, \beta_1} & V_{\alpha_{\downarrow}, \beta_2} \\ V_{\alpha_{\leftrightarrow}, \beta_1}^T & V_{\alpha_{\downarrow}, \beta_1}^T & V_{\beta_1} & V_{\beta_1, \beta_2} \\ V_{\alpha_{\leftrightarrow}, \beta_2}^T & V_{\alpha_{\downarrow}, \beta_2}^T & V_{\beta_1, \beta_2} & V_{\beta_2} \end{pmatrix}, \quad (10)$$

where V_μ and $V_{\mu\nu}$ are blocks of 2×2 matrices (with $\mu, \nu \equiv \alpha_p, \beta_j$). The covariance matrix elements can be analytically evaluated, but this leads to a tedious task, and to cumbersome expressions. Therefore, these expressions will be computed numerically instead. For simplicity and without loss of the generality, we assume that our mechanical resonators are degenerated, i.e., $\omega_j \equiv \omega_m$ and $\gamma_j \equiv \gamma_m$. We have used the following art-of-the-state optomechanical parameters [47, 48, 50, 51], i.e., $\omega_m/2\pi = 10\text{MHz}$; $\omega_1 = \omega_m$, $\omega_2 = \omega_m$, $\kappa = 0.2\omega_m$, $\Delta_p = -\omega_m$, $\gamma_m = 10^{-5}\omega_m$, $G_m = 0.2\omega_m$, and $J_m = 0.2\omega_m$. The phase θ and the angle ϕ are adjusted later on.

The diagonal blocks denoted as V_μ correspond to the optical modes ($\mu = \alpha_p$), and the mechanical mode ($\mu = \beta_j$), respectively. The off-diagonal blocks capture the correlations between different subsystems, i.e., V_{α_p, β_j} describes the correlations between the p^{th} intracavity field and the j^{th} mechanical mode. A bipartite entanglement within two subsystems can be quantified using the logarithmic negativity (E_N), which can be evaluated by tracing out the non-necessary modes. The logarithmic negativity E_N is defined as [52, 53],

$$E_N = \max[0, -\ln(2v^-)], \quad (11)$$

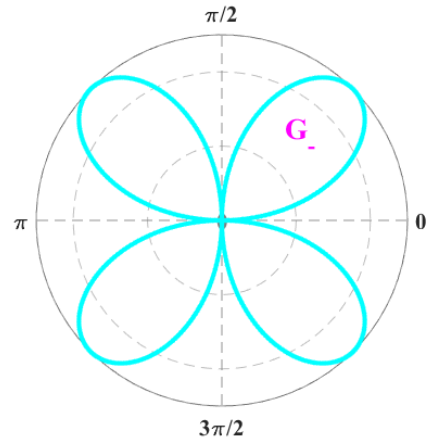


FIG. 3: (a) Coupling strength G_- in polar-coordinate versus the polarized angle ϕ for $G_m = 0.2\omega_m$, $\tilde{\Delta}_{\downarrow} = -\omega_m$, and $\tilde{\Delta}_{\leftrightarrow} = -(1 + 10^{-3})\omega_m$. The other parameters are $J_m = 0$, $\kappa = 0.2\omega_m$, $\omega_j = \omega_m$, and $\gamma_j = 10^{-5}\omega_m$.

where $v^- = \min \text{eig}[i\Omega_2\tilde{\chi}_4]$, with the symplectic matrix $\Omega_2 = \otimes_{j=1}^2 i\sigma_y$, and σ_y being the y -Pauli matrix. In this definition, v^- refers to the minimum symplectic eigenvalue of the covariant matrix $\tilde{\chi}_4 = P_{1|2}\chi_4 P_{1|2}$, where χ_4 is a 4×4 matrix of the targeted subsystems that is defined as,

$$\chi_4 = \begin{pmatrix} V_\mu & V_{\mu\nu} \\ V_{\mu\nu}^T & V_\nu \end{pmatrix}, \quad (12)$$

and $P_{1|2} = \text{diag}(1, -1, 1, 1)$ is a matrix that realizes partial transposition at the level of χ_4 . From Equation 11, there is an entanglement emerging from the system if and only if the condition $v^- < 1/2$ is fulfilled, which is equivalent to Simon's necessary and sufficient entanglement criterion for Gaussian states. Throughout the work, we consider the red-sideband detuning driving for the mechanical resonator ($\tilde{\Delta}_p = -\omega_m$), where sufficient heating processes are suppressed in the system.

In order to quantify tripartite entanglement, we compute the minimum residual contangle between each polarized mode and the two mechanical resonators. Therefore, we define $R^{\alpha_u|\beta_1|\beta_2}$ ($R^{\alpha_u|\beta_1|\beta_2}$) as the minimum residual contangle between TM (TE) mode with the two mechanical resonators $m_{j=1,2}$. For a given triplet of mode u, v, w , the minimum residual contangle is defined as [54, 55], $R^{u|v|w} = R^{u|(vw)} - R^{u|v} - R^{u|w}$, ($u, v, w \equiv \alpha_{h,v}, \beta_1, \beta_2$). In this formulation, $R^{u|v}$ stands for the contangle of subsystems labeled by u and v (where v can contain one or two modes), which is the squared logarithmic negativity. To evaluate the one-mode-vs-two-modes logarithmic negativity $R^{u|(vw)}$, one just needs to consider the definition of Equation 11 where we substitute the quantities $\Omega_2 = \otimes_{j=1}^2 i\sigma_y$ and $\tilde{\chi}_4 = P_{1|2}\chi_4 P_{1|2}$ with $\Omega_3 = \otimes_{j=1}^3 i\sigma_y$ and $\tilde{\chi}_6 = P_{u|vw}\chi_6 P_{u|vw}$, respectively. In these new definitions, χ_6 is 6×6 covariance matrix for the subsystem of interest, $P_{1|23} = \text{diag}(1, -1, 1, 1, 1, 1)$, $P_{2|13} =$

$\text{diag}(1, 1, 1, -1, 1, 1)$, and $P_{3|12} = \text{diag}(1, 1, 1, 1, 1, -1)$ are partial transposition matrices. To be a proper entanglement measure, the residual contangle must fulfill the monogamy of quantum entanglement, i.e., $R^{u|v|w} > 0$ that is similar to the Coffman-Kundu-Wootters monogamy inequality [56]. Therefore, the quantification of CV tripartite entanglement is, $R^{min} \equiv \min [R^{\alpha_{h,v}|\beta_1|\beta_2}, R^{\beta_1|\alpha_{h,v}|\beta_2}, R^{\beta_2|\alpha_{h,v}|\beta_1}]$, which ensures that the residual contangle R^{min} is invariant under all permutations of the modes resulting in a genuine three-way property of any three-mode Gaussian state.

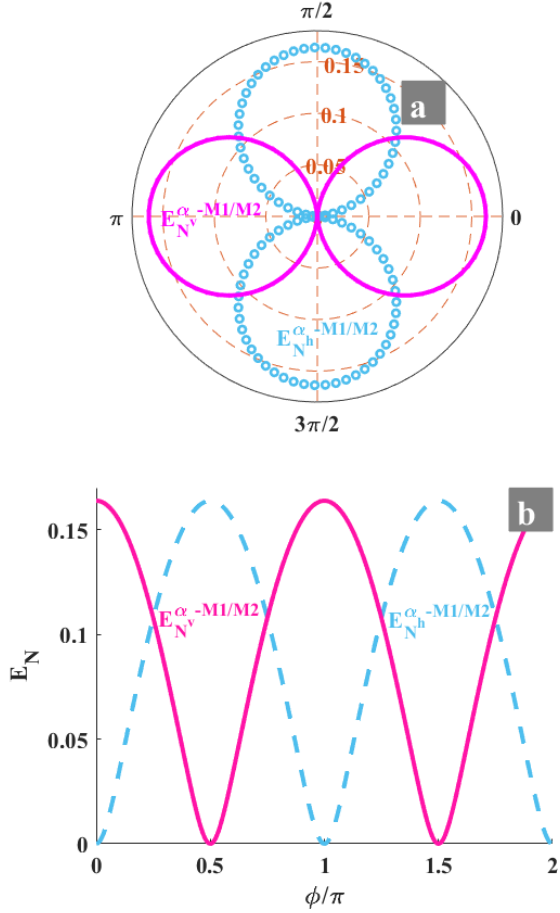


FIG. 4: (a) Polar entanglement representation and its (b) 2D-representation versus ϕ for $J_m = 0$. The quantity $E_N^{\alpha_{N^v}-M1/M2}$ ($E_N^{\alpha_{N^h}-M1/M2}$) is the bipartite entanglement between the TE (TM) mode and each mechanical resonator. In these figures, $G_m = 0.2\omega_m$, $n_{th}^j = 100$, and the other parameters are the same as in Figure 3.

III. ENHANCING BIPARTITE POLARIZATION ENTANGLEMENT VIA DARK MODE CONTROL

In this section, we aim to enhance bipartite entanglement in our system through dark mode control. For this purpose, we

consider our linearized Hamiltonian,

$$H_{lin}^r = - \sum_{p=\uparrow,\leftrightarrow} (\tilde{\Delta}_p + i\frac{\kappa}{2}) \delta\alpha_p^\dagger \delta\alpha_p + \sum_{j=1,2} (\omega_j - i\frac{\gamma_m}{2}) \delta\beta_j^\dagger \delta\beta_j + \sum_{j=1,2} \sum_{p=\uparrow,\leftrightarrow} G_p (\delta\alpha_p^\dagger \delta\beta_j + \delta\alpha_p \delta\beta_j^\dagger) + J_m (e^{i\theta} \delta\beta_1^\dagger \beta_2 + e^{-i\theta} \beta_1 \beta_2^\dagger). \quad (13)$$

By assuming no coupling between the mechanical resonators ($J_m = 0$), and by defined the following bosonic bright and dark modes,

$$\begin{cases} \delta\alpha_{\leftrightarrow} &= \frac{G_{\leftrightarrow} B_+ + G_{\uparrow} B_-}{G}, \\ \delta\alpha_{\uparrow} &= \frac{G_{\uparrow} B_+ - G_{\leftrightarrow} B_-}{G}, \end{cases} \quad (14)$$

where $G = \sqrt{G_{\uparrow}^2 + G_{\leftrightarrow}^2}$, this linearized Hamiltonian can be re-written in terms of bright and dark modes as,

$$H_{lin}^r = - \sum_{k=\pm} \omega_k B_k^\dagger B_k - G_+ \sum_{j=1,2} (\delta\beta_j B_+^\dagger + \delta\beta_j^\dagger B_+) + \sum_{j=1,2} (\omega_j - i\frac{\gamma_m}{2}) \delta\beta_j^\dagger \delta\beta_j + G_- (B_+^\dagger B_- + B_+^\dagger B_-), \quad (15)$$

with $G_+ = G$, $G_- = \frac{G_{\uparrow} G_{\leftrightarrow}}{|G|^2} (\tilde{\Delta}_{\leftrightarrow} - \tilde{\Delta}_{\uparrow})$, and $\omega_{\pm} = \frac{(\tilde{\Delta}_{\uparrow} + i\frac{\kappa}{2}) |G_{\leftrightarrow(\uparrow)}|^2 + (\tilde{\Delta}_{\leftrightarrow} + i\frac{\kappa}{2}) |G_{\uparrow(\leftrightarrow)}|^2}{|G|^2}$. From Equation 15 and the expressions of G_{\pm} , it can be seen that $G_- = 0$ for $\tilde{\Delta}_{\leftrightarrow} = \tilde{\Delta}_{\uparrow}$, and that leads to the fact that the mode B_- is decoupled from the system, i.e., it is a dark mode. Moreover, this dark mode can be also displayed by controlling the polarization angle ϕ . Indeed, for $\tilde{\Delta}_{\leftrightarrow} \neq \tilde{\Delta}_{\uparrow}$, dark mode shows up for either $G_{\uparrow} = 0$ (for $\phi = \frac{\pi}{2}n$ with n an odd integer) or $G_{\leftrightarrow} = 0$ (for $\phi = n\pi$ with n an integer). Beside of this dark mode, one has the bright mode B_+ which is always coupled to the mechanical mode owing to $G_+ > 0$ as long as $G_m \neq 0$. In Figure 3, we have displayed the coupling G_- in ϕ -polar representation. As predicted, it can be seen that dark mode exists for $\phi = \frac{\pi}{2}n$ with n an integer, even though $\tilde{\Delta}_{\uparrow} \neq \tilde{\Delta}_{\leftrightarrow}$. Therefore, the Optical Dark Mode Unbreaking (ODMU) regime corresponds to $\phi = \frac{\pi}{2}n$ with n an integer, while Optical Dark Mode breaking (ODMB) happens when $\phi \neq \frac{\pi}{2}n$ with n an integer. Such dark mode control based on the polarization angle, while the cavities are non-degenerated, is one of the key points of our investigation, because it reflects the physical case where engineering degenerated cavities is a difficult task. When the phonon hopping rate is non zero ($J_m \neq 0$), each polarized field couples with the two coupled mechanical resonators. In this case, our system can be reduced to the one investigated in [34] where dark mode is controlled via the modulation phase of J_m . However, we are mostly interested in the dark mode control via the polarization angle in our investigation here, since it is the one that induces multi-path entanglement.

The investigated bipartite entanglement is displayed in Figure 4, for $J_m = 0$. Figure 4a depicts the polar representation of the entanglement between the TE (TM) mode and one of the mechanical resonators, i.e., $E_N^{\alpha_{N^v}-M1/M2}$ ($E_N^{\alpha_{N^h}-M1/M2}$). It

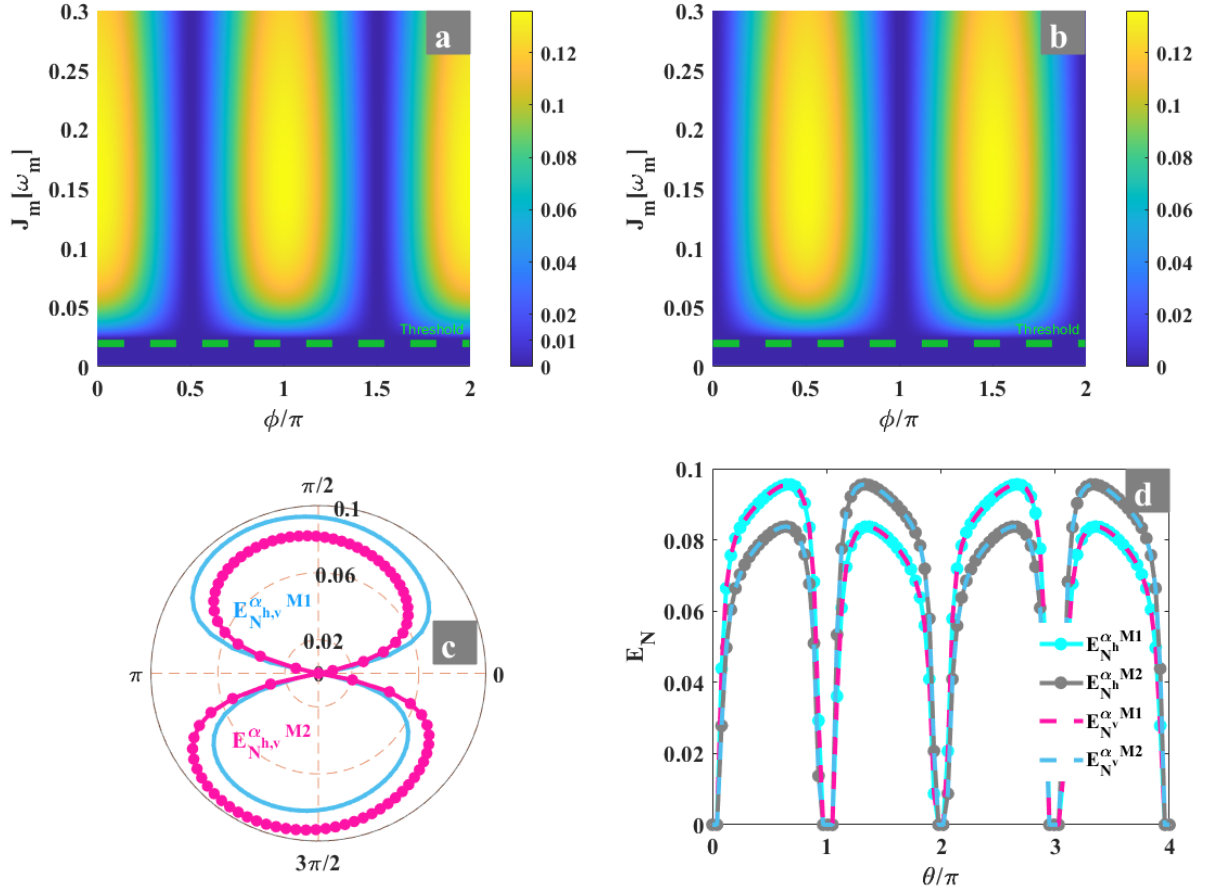


FIG. 5: (a) Contour plot of the entanglement between TE mode and each mechanical resonator ($E_N^{\alpha_h-M1/M2}$) versus J_m and ϕ for $\theta = \frac{\pi}{2}$. (b) Contour plot of the entanglement between TM mode and each mechanical resonators ($E_N^{\alpha_h-M1/M2}$) versus J_m and ϕ for $\theta = \frac{\pi}{2}$. (c) Polar entanglement representation versus θ for $J_m = 0.2\omega_m$ and $\phi = \frac{\pi}{4}$. (d) 2D-representation of (c) where $E_N^{\alpha_h-M1}$ ($E_N^{\alpha_h-M2}$) reaches its optimal value for $\theta = (n+1/2)\pi$, n being an even integer ($\theta = (n+1/2)\pi$, n being an odd integer). For all these figures, $G_m = 0.2\omega_m$, $n_{th}^j = 100$, and the other parameters are the same as in Figure 3.

can be seen that the entanglement $E_N^{\alpha_v-M1/M2}$ (solid line in Figure 4a) reach its optimal value for $\phi = n\pi$ with n being an integer. One also observes that this entanglement does not exist ($E_N^{\alpha_v-M1/M2} = 0$) for $\phi = m\frac{\pi}{2}$ with m being an odd integer. Reversely, the entanglement $E_N^{\alpha_h-M1/M2}$ (dotted line in Figure 4a) has its optimal values at $\phi = m\frac{\pi}{2}$ with m being an odd integer, while it vanishes ($E_N^{\alpha_h-M1/M2} = 0$) for $\phi = n\pi$ with n being an integer. This behavior of $E_N^{\alpha_v-M1/M2}$ ($E_N^{\alpha_h-M1/M2}$) is related to the polarization feature used, since the TE (TM) mode does not exist for $\phi = n\pi$ ($\phi = m\frac{\pi}{2}$) as aforementioned. Moreover, it can be seen that the same amount of these entanglement simultaneously exist at $\phi = (p+1)\frac{\pi}{4}$ for p and even integer, resulting to fact that four entanglement paths are engineered in our system simultaneously. Such feature of multi-path entanglement in our proposal is triggered by the polarization effect, which constitutes the merit of introducing polarized fields in our investigation. These features of $E_N^{\alpha_v-M1/M2}$

and $E_N^{\alpha_h-M1/M2}$ can be also displayed in 2-D-representation as depicted in Figure 4b, where these same quantities are shown versus the polarized angle ϕ . One can observe that the generated entanglements exhibit oscillatory behaviors, which are reminiscent of entanglement death and revival phenomena. From the above observation, it results that only TE ($E_N^{\alpha_v-M1/M2}$) entanglement or TM ($E_N^{\alpha_h-M1/M2}$) entanglement exists in the ODMU regime. In order to simultaneously generate these entanglement, the dark mode must be broken by adjusting $\phi \neq \frac{\pi}{2}n$ leading to the ODMB regime where four entanglement quantities are engineered. This multi-path entanglement engineering is fully based on the polarization angle ϕ together with dark mode control.

The bipartite entanglement feature in our proposal can be further impacted as the mechanical coupling came into play ($J_m \neq 0$). In Figure 5, the entanglement is displayed when the dark mode effect is broken, i.e., $J_m \neq 0$ and $\theta = \pi/2$. For instance, Figure 5a (Figure 5b) depicts the contour plot

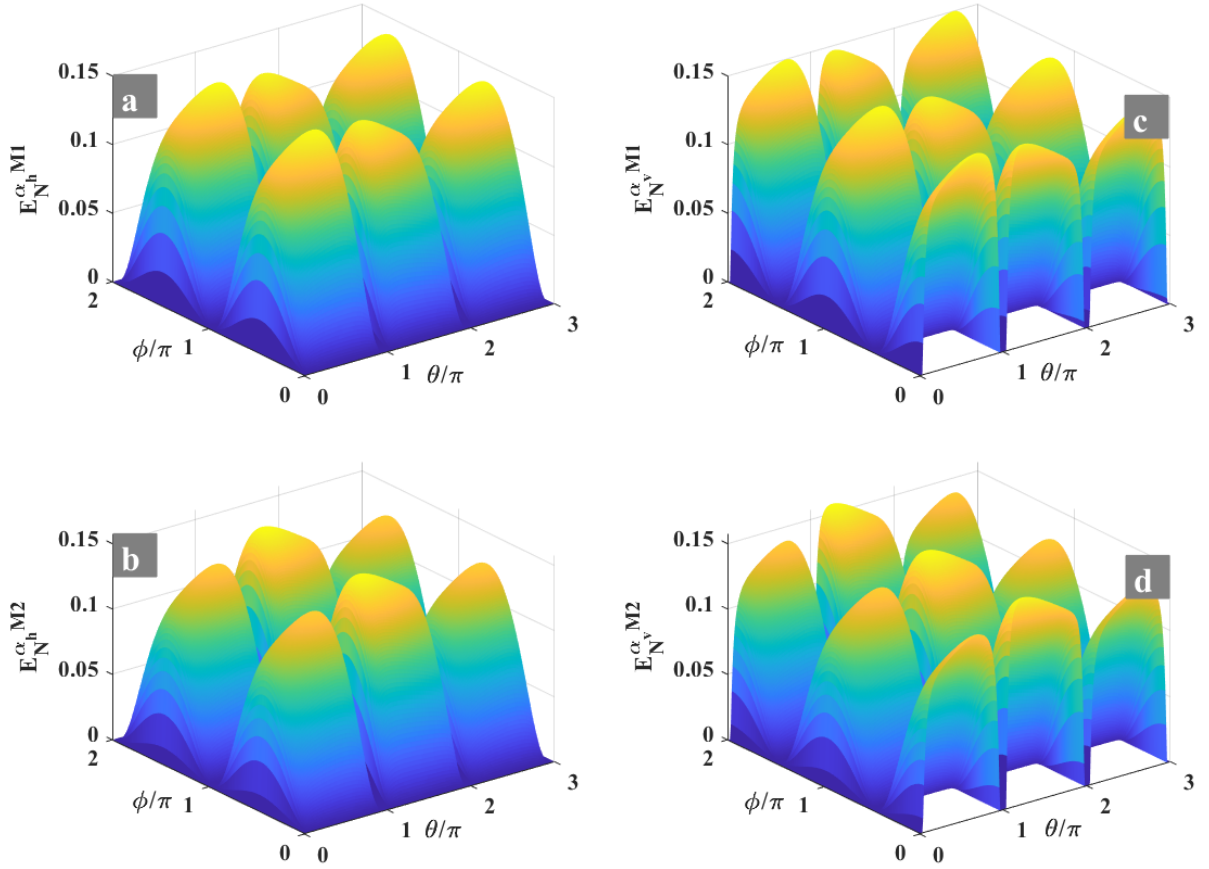


FIG. 6: 3D-representation of the entanglements versus the polarization angle ϕ and the modulation phase θ . (a,b) Entanglement between the TM polarized mode with the first ($E_N^{\alpha_h-M1}$) and second ($E_N^{\alpha_h-M2}$) mechanical resonator, respectively. (c,d) Entanglement involving the TE polarized mode with the first ($E_N^{\alpha_v-M1}$) and second ($E_N^{\alpha_v-M2}$) mechanical resonator. For these figures, we have set $n_{th}^j = 100$, $J_m = 0.2\omega_m$ and $G_m = 0.2\omega_m$. The other parameters are the same as in Figure 3.

of $E_N^{\alpha_v-M1/M2}$ ($E_N^{\alpha_h-M1/M2}$) versus the coupling J_m and the polarization angle ϕ for $\theta = \pi/2$. It can be seen that the TE (TM) mode is optimally entangled to the mechanical resonators for $\phi = n\pi$ with n being an integer ($\phi = n\frac{\pi}{2}$ with n being an odd integer). Moreover, these entanglements are generated from a certain threshold of the phonon hopping rate, i.e., $J_m \gtrsim 0.05\omega_m$. To point out the entanglement feature over the phase-dependent mechanical coupling, we plotted the polar representation of the entanglement versus θ in Figure 5c for $\phi = \pi/4$ and $J_m = 0.2\omega_m$. It can be seen that the entanglement between each polarized mode and the first mechanical resonator $E_N^{\alpha_{h,v}-M1}$ (second mechanical resonator $E_N^{\alpha_{h,v}-M2}$) reaches its optimal value for $\phi = (2n+1)\frac{\pi}{2}$ with n being an even integer ($\phi = (2n+1)\frac{\pi}{2}$ with n being an odd integer). Moreover, it is interesting to mention that there is an switching between these entanglements depending on whether we are on the upper half or the lower half of the unit circle. This switching can be further observed in Figure 5d, which displays entanglement versus θ with the same parameters as in Figure 5c.

In order to investigate both effect of ϕ and θ on the bipartite entanglement, we displayed on Figure 6 a plot of the entanglements versus ϕ and θ . Indeed, Figure 6(a-d) represent the entanglement between the TM mode with first mechanical resonator ($E_N^{\alpha_h-M1}$), the TE mode with first mechanical resonator ($E_N^{\alpha_v-M1}$), the TM mode with second mechanical resonator ($E_N^{\alpha_h-M2}$), and the TE mode with second mechanical resonator ($E_N^{\alpha_v-M2}$), respectively. It can be observed that under the dark mode breaking condition ($\theta = n\frac{\pi}{2}$ with n being an odd integer) the entanglements involving TM mode reached their optimal values for $\phi = (2n+1)\frac{\pi}{2}$ with n being an even integer, while those involving the TE mode are maximum for $\phi = n\pi$ with n being an integer. Moreover, the peaks of these entanglements are not equivalently distributed depending on when the mode TM or TE is coupled to the first or second resonator. For instance, the peaks appearing on Figure 6a and Figure 6b are not similarly distributed even though both entanglements involve TM. This also applies to Figure 6c and Figure 6d for TE mode. This reveals that the interaction between the polarized modes and the mechanical resonators does not necessary

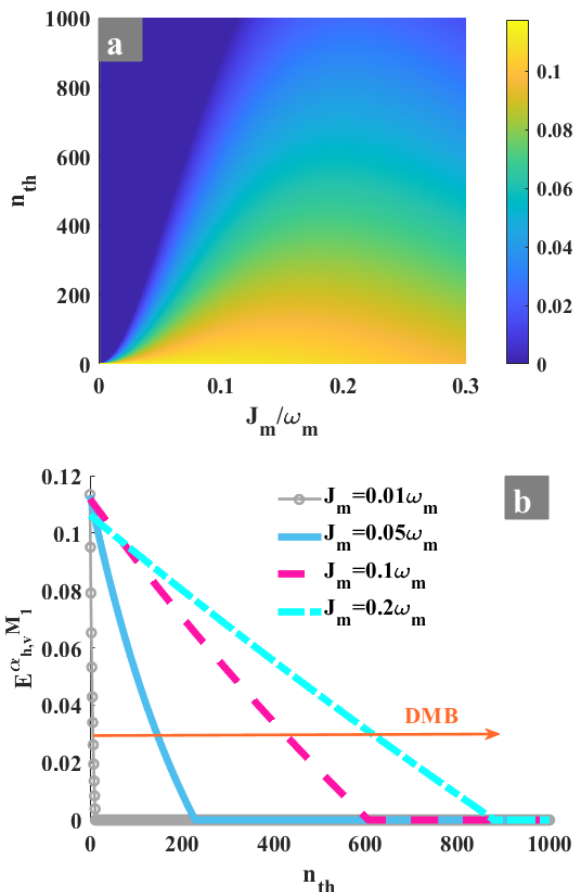


FIG. 7: (a) Contour plot of the entanglement $E_N^{\alpha_h, v, M1}$ versus J_m and the thermal phonon number n_{th} for $G_m = 0.2\omega_m$, $\phi = \pi/4$, and $\theta = \pi/2$. (b) Corresponding 2D-representation of (a) with different values of J_m , under the DMB regime condition. The other parameters are as those in Figure 3.

leads to symmetric entanglements. This asymmetric of the entanglement further highlight the multi-entanglement path feature in our system. Thermal management of these generated bipartite entanglement is carried out in Figure 7. A contour plot of the entanglement $E_N^{\alpha_h, v, M1}$ versus the coupling J_m and the thermal phonon number n_{th} is displayed in Figure 7a, for $\theta = \pi/2$. It can be seen that the entanglement survives longer against thermal noise as the coupling J_m increases. For weak strength of the mechanical coupling ($J_m < 0.01\omega_m$), the generated entanglement is so fragile and disappears for few thermal phonons ($n_{th} \sim 10$). Therefore, it results that the breaking of the dark mode significantly improves the resilience of the entanglement against thermal fluctuations. This can be further seen in Figure 7b, where almost two order of magnitude of robustness against thermal noise is reached under dark mode control. Such a thermal management of quantum entanglement is useful for engineering noise-tolerant quantum correlations which are vital resources for modern quantum applications.

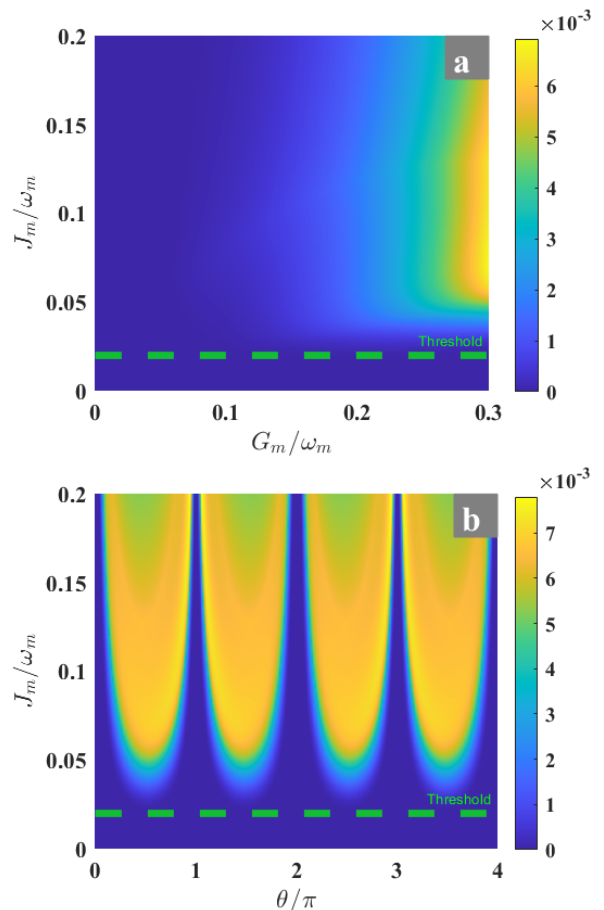


FIG. 8: (a) Contour plot of the residual cotangle $R_{\alpha_h}^{min}$ (same for $R_{\alpha_v}^{min}$) versus J_m and G_m for $\phi = \pi/4$, $\theta = \pi/2$. (b) Contour plot of the residual cotangle $R_{\alpha_h}^{min}$ (same for $R_{\alpha_v}^{min}$) versus J_m and θ for $\phi = \pi/4$, $G_m = 0.3\omega_m$, and $n_{th}^j = 100$. The green dashed line indicates the threshold value of $J_m \sim 0.02\omega_m$ from which tripartite entanglement is generated. The other parameters are as those in Figure 3.

IV. ENGINEERING TRIPARTITE POLARIZATION ENTANGLEMENT VIA DARK MODE CONTROL

In this section, we investigate tripartite entanglement in our system. For this purpose, we seek to compute the minimum residual cotangle between each polarized mode and the two mechanical resonators, as a mean of quantifying tripartite entanglement. For simplicity in our notations, we define $R_{\alpha_h}^{min}$ ($R_{\alpha_v}^{min}$) as the minimum residual cotangle between TM (TE) mode with the two mechanical resonators. As we intend to generate multi-path tripartite entanglement, the polarization angle ϕ and the breaking of the dark mode through θ (or J_m) will be our parameters of interests. Moreover, we have checked and found that tripartite entanglement involving the two polarized fields and any of the mechanical resonators does not exist or is irrelevant (not shown here).

In Figure 8, we represent contour plot of residual cotangle versus J_m and G_m (Figure 8 a) and versus J_m and θ (Fig-

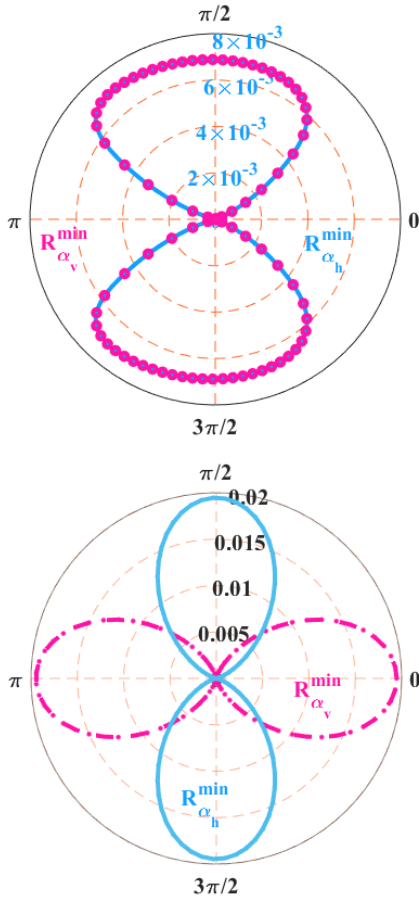


FIG. 9: (a) Polar representation of the residual cotangle $R_{\alpha_h}^{\min}$ (same for $R_{\alpha_v}^{\min}$) versus θ for $\phi = \pi/4$. (b) Polar representation of the residual cotangle $R_{\alpha_v}^{\min}$ (same for $R_{\alpha_h}^{\min}$) versus ϕ for $\theta = \pi/2$. For these plots, we have set $J_m = 0.08\omega_m$, $G_m = 0.3\omega_m$ and $n_{th}^j = 100$. The other parameters are as those in Figure 3.

ure 8 b). As expected, tripartite entanglement is generated in our proposal only when $J_m \neq 0$ and this is shown through the green threshold line in Figure 8a ($J_m \sim 0.022\omega_m$). Moreover, it can be also observed that the generated tripartite entanglement requires also a threshold for the driving coupling strength $G_m \sim 0.15\omega_m$. Furthermore, this entanglement is generated when $\theta \neq n\pi$ with n being an integer (Figure 8 b). Therefore, it results that tripartite entanglement is generated in our system under the dark mode breaking condition. It is worth mentioning that the polarization angle is set to $\phi = \pi/4$ in Figure 8, leading to the fact that both $R_{\alpha_h}^{\min}$ and $R_{\alpha_v}^{\min}$ are similar. To further get insight about the effect of both ϕ and θ on the generated residual cotangle, we displayed tripartite entanglement in polar representation in Figure 9. The tripartite entanglement is depicted versus θ (ϕ) in Figure 9a (Figure 9b). It can be seen that entanglement is generated only under the dark mode breaking condition ($\theta \neq n\pi$), and reaches its maximum value around $\theta = m\pi/2$, with m being an odd integer. Moreover, the quantities $R_{\alpha_h}^{\min}$ and $R_{\alpha_v}^{\min}$ are similar as

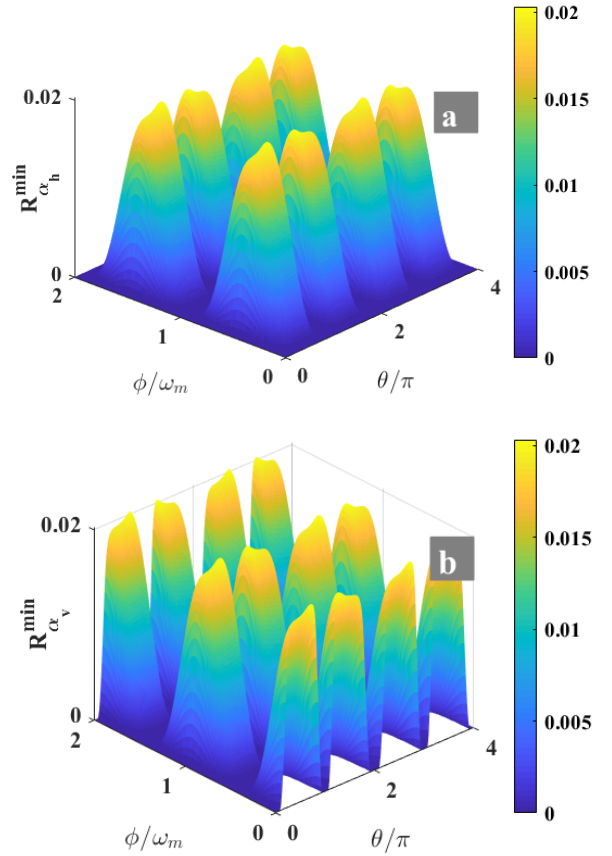


FIG. 10: (a) Residual cotangle $R_{\alpha_h}^{\min}$ and (b) $R_{\alpha_v}^{\min}$ versus ϕ and θ for $J_m = 0.08\omega_m$, $G_m = 0.3\omega_m$ and $n_{th}^j = 100$. The other parameters are as those in Figure 3.

aforementioned (for $\phi = \pi/4$). This is displayed in Figure 9b, which captures a polar representation of the entanglement versus ϕ . It can be observed that both entanglements $R_{\alpha_h}^{\min}$ and $R_{\alpha_v}^{\min}$ perfectly hybridize at $\phi = \pi/4$, while $R_{\alpha_h}^{\min}$ ($R_{\alpha_v}^{\min}$) is optimal for $\phi = m\pi/2$, with m being an odd integer ($\phi = n\pi$, with n being any integer). From Figure 8 and Figure 9, it results that tripartite entanglement is generated in our system only in the dark mode broken regime ($J_m \neq 0$, $\theta \neq n\pi$). Furthermore, multi-path entanglement triggers in the system under the condition $\phi \neq p\pi/2$, p being any integer. Such multi-path tripartite entanglement generation can be useful for quantum information processing and diverse quantum computational tasks. This multi-path entanglement engineering can be further fostered by displaying entanglement versus θ and ϕ as shown in Figure 10. Indeed, as it can be seen in Figure 10a and Figure 10b, different patterns of tripartite entanglements are displayed depending on the value of both θ and ϕ . The residual cotangle involving the TM (TE) mode with the two mechanical resonators results to different patterns where the entanglement peaks show up either at $\phi = p\pi/2$, p being an odd integer for $R_{\alpha_h}^{\min}$ (see Figure 10a), or at $\phi = m\pi$, m being any integer for $R_{\alpha_v}^{\min}$ (see Figure 10b). Therefore, the polarization

angle ϕ is revealed as a key parameter that induces multi-paths entanglement features in our system, which provides a way to access abundant tripartite quantum resources to boost number of quantum applications including quantum information processing, quantum computation and other quantum tasks.

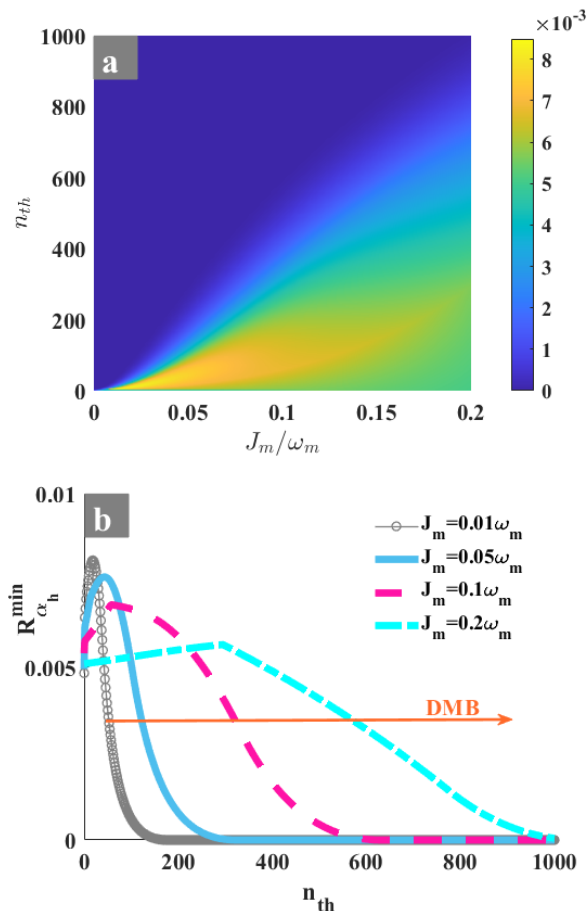


FIG. 11: (a) Contour plot of the residual cotangle $R_{\alpha_h}^{min}$ (same for $R_{\alpha_v}^{min}$) versus thermal phonon number n_{th} and J_m for $\phi = \pi/4$, $\theta = \pi/2$ and $G_m = 0.3\omega_m$. The other parameters are as those in Figure 3.

Another interesting property of the residual cotangle to figure out is its robustness against thermal fluctuations. This feature reveals how strong the generated entanglement can resist to thermal bath, and this is interesting for number of open systems which interact with their environment. Figure 11 displays contour plot of residual cotangle versus the thermal phonon number (n_{th}) and the phonon hopping rate J_m . It can be seen that the tripartite entanglement resists more to thermal fluctuation as the coupling J_m is increases (see Figure 11a). This further highlights the merit of having $J_m \neq 0$ in our system, because $J_m = 0$ does not lead to any entanglement in our proposal. Moreover, Figure 11 depicts how the entanglement is triggered in the dark mode breaking regime, as indicated through direction of the arrow, and this entanglement resists to a thermal phonon population of $n_{th} \sim 1000$, which is up to two order of magnitude stronger than in the Unbreaking regime. It

is noteworthy to mention that we have set $\phi = n\pi/4$ in Figure 11, so that the plots capture both $R_{\alpha_h}^{min}$ and $R_{\alpha_v}^{min}$ which are equivalent. Such a noise-tolerant entanglement is suitable for number of modern quantum applications.

V. CONCLUSION

We have proposed a scheme to engineer multi-path entanglements in optomechanical system through dark mode control. Our model consists of vector electromagnetic fields, i.e., the vertical (transverse electric (TE) and horizontal (transverse magnetic [(TM]) modes, which drive two mechanically coupled mechanical resonators. The phase modulation of the mechanical coupling (θ) together with the polarization angle (ϕ) are used to switch from the dark mode unbroken to the dark mode broken regimes in our proposal. When the mechanical coupling is turned off ($J_m = 0$), only bipartite multi-path entanglements are generated under dark mode control through the polarization angle. For $J_m \neq 0$ the dark mode breaking depends on simultaneous tuning of both θ and ϕ , leading to an engineering of both multi-path bipartite and tripartite entanglements in the system. The engineered entanglements are triggered from a certain threshold of the mechanical coupling, and are enhanced as the strength of J_m increases. For specific value of the polarization angle $\phi = \pi/4$, twin entangled states are generated, which might be useful for particular tasks and technological applications. Moreover, the generated entangled states are more resilient against thermal fluctuations in the DMB regime, i.e., at least two order of magnitude of robustness enhancement against thermal phonon population is achieved compared to the Unbreaking regime. The multi-path entanglement generation scheme introduced in this work reveals how noise-tolerant quantum resources can be engineered in optomechanical system, and such resources can be useful for quantum information processing, quantum communication, and number of quantum computational tasks. Furthermore, the proposed scheme can be extended to other fields such as in microwave and hybrid optomechanical contexts.

Availability of data and materials

Relevant data are included in the manuscript, and supplement data are available upon reasonable request.

Competing interests

The authors declare that they have no competing interests.

Funding

Not applicable.

Authors' contributions

P. D. Conceptualized the work, carried out the simulations and wrote the original draft. **R. A.** Revised the draft and validated the numerical results. **A. J.A.:** Participated on the data curation and the validation of the results. **A. A.-K.:** Proposed the methodology, and revised the last version of the manuscript. **A.-H. A.-A.:** Supervised the work and participated on the revision and writing of the manuscript. All authors participated in the discussions.

Acknowledgments

P.D. acknowledges the Iso-Lomso Fellowship from the Stellenbosch Institute for Advanced Study (STIAS), Stellenbosch 7600, South Africa, and The Institute for Advanced Study, Wissenschaftskolleg zu Berlin, Wallotstrasse 19, 14193 Berlin, Germany. This work was supported by Princess Nourah bint Abdulrahman University Researchers Supporting Project number (PNURSP2026R399), Princess Nourah bint Abdulrahman University, Riyadh, Saudi Arabia. The authors are thankful to the Deanship of Graduate Studies and Scientific Research at the University of Bisha for supporting this work through the Fast-Track Research Support Program.

-
- [1] S. Slussarenko and G. J. Pryde, *Applied Physics Reviews* **6**, 041303 (2019), ISSN 1931-9401.
- [2] G. Wendin, *Reports on Progress in Physics* **80**, 106001 (2017), ISSN 1361-6633.
- [3] L. Pezzè, A. Smerzi, M. K. Oberthaler, R. Schmied, and P. Treutlein, *Reviews of Modern Physics* **90**, 035005 (2018), ISSN 1539-0756.
- [4] E. Polino, M. Valeri, N. Spagnolo, and F. Sciarrino, *AVS Quantum Science* **2**, 024703 (2020), ISSN 2639-0213.
- [5] C. Degen, F. Reinhard, and P. Cappellaro, *Reviews of Modern Physics* **89**, 035002 (2017), ISSN 1539-0756.
- [6] P. Djorwe, Y. Pennec, and B. Djafari-Rouhani, *Physical Review Applied* **12**, 024002 (2019), ISSN 2331-7019.
- [7] P. Djorwé, M. Asjad, Y. Pennec, D. Dutykh, and B. Djafari-Rouhani, *Physical Review Research* **6**, 033284 (2024), ISSN 2643-1564.
- [8] S. M. Tchounda, P. Djorwé, S. N. Engo, and B. Djafari-Rouhani, *Physical Review Applied* **19**, 064016 (2023), ISSN 2331-7019.
- [9] K. Stannigel, P. Rabl, A. S. Sørensen, P. Zoller, and M. D. Lukin, *Physical Review Letters* **105**, 220501 (2010), ISSN 1079-7114.
- [10] C. M. Knaut, A. Suleymanzade, Y.-C. Wei, D. R. Assumpcao, P.-J. Stas, Y. Q. Huan, B. Machielse, E. N. Knall, M. Sutula, G. Baranes, et al., *Nature* **629**, 573 (2024), ISSN 1476-4687.
- [11] S. Kucera, C. Haen, E. Arenskötter, T. Bauer, J. Meiers, M. Schäfer, R. Boland, M. Yahyapour, M. Lessing, R. Holzwarth, et al., *npj Quantum Information* **10**, 88 (2024), ISSN 2056-6387.
- [12] S. McArdle, S. Endo, A. Aspuru-Guzik, S. C. Benjamin, and X. Yuan, *Reviews of Modern Physics* **92**, 015003 (2020), ISSN 1539-0756.
- [13] K. Bharti, A. Cervera-Lierta, T. H. Kyaw, T. Haug, S. Alperin-Lea, A. Anand, M. Degroote, H. Heimonen, J. S. Kottmann, T. Menke, et al., *Reviews of Modern Physics* **94**, 015004 (2022), ISSN 1539-0756.
- [14] S. Bartolucci, P. Birchall, H. Bombín, H. Cable, C. Dawson, M. Gimeno-Segovia, E. Johnston, K. Kieling, N. Nickerson, M. Pant, et al., *Nature Communications* **14**, 912 (2023), ISSN 2041-1723.
- [15] P. S. Shah, F. Yang, C. Joshi, and M. Mirhosseini, *PRX Quantum* **5**, 030346 (2024), ISSN 2691-3399.
- [16] C. Chen, K. Tang, Y. Zhou, K. Yi, X. Zhang, X. Zhang, H. Guo, S. Liu, Y. Chen, T. Yan, et al., *Physical Review Research* **7**, L022018 (2025), ISSN 2643-1564.
- [17] F. Dieleman, M. S. Tame, Y. Sonnefraud, M. S. Kim, and S. A. Maier, *Nano Letters* **17**, 7455 (2017), ISSN 1530-6992.
- [18] B. Hensen, H. Bernien, A. E. Dréau, A. Reiserer, N. Kalb, M. S. Blok, J. Ruitenberg, R. F. L. Vermeulen, R. N. Schouten, C. Abellán, et al., *Nature* **526**, 682 (2015), ISSN 1476-4687.
- [19] M. Steffen, M. Ansmann, R. C. Bialczak, N. Katz, E. Lucero, R. McDermott, M. Neeley, E. M. Weig, A. N. Cleland, and J. M. Martinis, *Science* **313**, 1423 (2006), ISSN 1095-9203.
- [20] L. DiCarlo, M. D. Reed, L. Sun, B. R. Johnson, J. M. Chow, J. M. Gambetta, L. Frunzio, S. M. Girvin, M. H. Devoret, and R. J. Schoelkopf, *Nature* **467**, 574 (2010), ISSN 1476-4687.
- [21] T. A. Palomaki, J. D. Teufel, R. W. Simmonds, and K. W. Lehnert, *Science* **342**, 710 (2013), ISSN 1095-9203.
- [22] P. Chen, D.-W. Luo, and T. Yu, *Physical Review Research* **7** (2025), ISSN 2643-1564.
- [23] D. Vitali, S. Gigan, A. Ferreira, H. R. Böhm, P. Tombesi, A. Guerreiro, V. Vedral, A. Zeilinger, and M. Aspelmeyer, *Physical Review Letters* **98**, 030405 (2007), ISSN 1079-7114.
- [24] C. F. Ockelo-en-Korppi, E. Damskäg, J.-M. Pirkkalainen, M. Asjad, A. A. Clerk, F. Massel, M. J. Woolley, and M. A. Sillanpää, *Nature* **556**, 478 (2018), ISSN 1476-4687.
- [25] S. Kotler, G. A. Peterson, E. Shojaei, F. Lecocq, K. Cicak, A. Kwiatkowski, S. Geller, S. Glancy, E. Knill, R. W. Simmonds, et al., *Science* **372**, 622 (2021), ISSN 1095-9203.
- [26] L. Mercier de Lépinay, C. F. Ockelo-en-Korppi, M. J. Woolley, and M. A. Sillanpää, *Science* **372**, 625 (2021), ISSN 1095-9203.
- [27] D. R. K. Massembele, P. Djorwé, A. K. Sarma, A.-H. Abdel-Aty, and S. G. N. Engo, *Physical Review A* **110**, 043502 (2024), ISSN 2469-9934.
- [28] Z.-B. Yang, J.-S. Liu, H. Jin, Q.-H. Zhu, A.-D. Zhu, H.-Y. Liu, Y. Ming, and R.-C. Yang, *Optics Express* **28**, 31862 (2020), ISSN 1094-4087.
- [29] P. Djorwé, A.-H. Abdel-Aty, K. Nisar, and S. Engo, *Optik* **319**, 172097 (2024), ISSN 0030-4026.
- [30] D. Massembele, P. Djorwé, K. Emale, J.-X. Peng, A.-H. Abdel-Aty, and K. Nisar, *Physica B: Condensed Matter* **697**, 416689 (2025), ISSN 0921-4526.
- [31] N. Ghorbani, A. Motazedifard, and M. H. Naderi, *Physical Re-*

- view A **111**, 013524 (2025), ISSN 2469-9934.
- [32] Z. Li, X. Li, and X. Zhong, *Optics Express* **31**, 19382 (2023), ISSN 1094-4087.
- [33] D.-G. Lai, Y.-H. Chen, W. Qin, A. Miranowicz, and F. Nori, *Physical Review Research* **4**, 033112 (2022), ISSN 2643-1564.
- [34] D.-G. Lai, J.-Q. Liao, A. Miranowicz, and F. Nori, *Physical Review Letters* **129**, 063602 (2022), ISSN 1079-7114.
- [35] A. Rossi, G. Vallone, A. Chiuri, F. De Martini, and P. Mataloni, *Physical Review Letters* **102**, 153902 (2009), ISSN 1079-7114.
- [36] L. Zhang and Q. Liu, *Quantum Information Processing* **22**, 148 (2023), ISSN 1573-1332.
- [37] V. Mannalath and A. Pathak, *Physical Review A* **108**, 062614 (2023), ISSN 2469-9934.
- [38] E. Sutcliffe and A. Beghelli, *IEEE Transactions on Quantum Engineering* **4**, 1 (2023), ISSN 2689-1808.
- [39] X.-M. Hu, W.-B. Xing, B.-H. Liu, Y.-F. Huang, C.-F. Li, G.-C. Guo, P. Erker, and M. Huber, *Physical Review Letters* **125**, 090503 (2020), ISSN 1079-7114.
- [40] R. Duggan, J. del Pino, E. Verhagen, and A. Alù, *Physical Review Letters* **123**, 023602 (2019), ISSN 1079-7114.
- [41] D. Oh, S. Baek, S. Lee, K. Lee, J. Park, Z. Liu, T.-T. Kim, and B. Min, *Nanophotonics* **13**, 4409 (2024), ISSN 2192-8614.
- [42] W. P. Bowen, N. Treps, R. Schnabel, and P. K. Lam, *Physical Review Letters* **89**, 253601 (2002), ISSN 1079-7114.
- [43] H. Xiong, Y.-M. Huang, L.-L. Wan, and Y. Wu, *Physical Review A* **94**, 013816 (2016), ISSN 2469-9934.
- [44] B. Wang, H. Xiong, X. Jia, and Y. Wu, *Scientific Reports* **8**, 282 (2018), ISSN 2045-2322.
- [45] F. M. Buters, M. J. Weaver, H. J. Eerkens, K. Heeck, S. de Man, and D. Bouwmeester, *Physical Review A* **94**, 063813 (2016), ISSN 2469-9934.
- [46] Y. Li, Y.-F. Jiao, J.-X. Liu, A. Miranowicz, Y.-L. Zuo, L.-M. Kuang, and H. Jing, *Nanophotonics* **11**, 67 (2021), ISSN 2192-8614.
- [47] J. P. Mathew, J. d. Pino, and E. Verhagen, *Nature Nanotechnology* **15**, 198 (2020), ISSN 1748-3395.
- [48] J. J. Slim, J. del Pino, and E. Verhagen, *Nature Communications* **16**, 7471 (2025), ISSN 2041-1723.
- [49] E. X. DeJesus and C. Kaufman, *Physical Review A* **35**, 5288 (1987), ISSN 0556-2791.
- [50] K. Fang, J. Luo, A. Metelmann, M. H. Matheny, F. Marquardt, A. A. Clerk, and O. Painter, *Nature Physics* **13**, 465 (2017), ISSN 1745-2481.
- [51] C. Brendel, V. Peano, O. J. Painter, and F. Marquardt, *Proceedings of the National Academy of Sciences* **114**, E3390 (2017), ISSN 1091-6490.
- [52] G. Vidal and R. F. Werner, *Physical Review A* **65**, 032314 (2002), ISSN 1094-1622.
- [53] M. B. Plenio, *Physical Review Letters* **95**, 090503 (2005), ISSN 1079-7114.
- [54] G. Adesso and F. Illuminati, *New Journal of Physics* **8**, 15 (2006), ISSN 1367-2630.
- [55] G. Adesso and F. Illuminati, *Journal of Physics A: Mathematical and Theoretical* **40**, 7821 (2007), ISSN 1751-8121.
- [56] V. Coffman, J. Kundu, and W. K. Wootters, *Physical Review A* **61**, 052306 (2000), ISSN 1094-1622.